Available online at www.sciencedirect.com
SCIENCE DIRECT
Journal of Photochemistry and Photobiology A: Chemistry 175 (2005) 192–200
Journal of Photochemistry and Photobiology A:Chemistry
www.elsevier.com/locate/jphotochem

On the mechanism of TiO_2-photocatalyzed degradation of aniline derivatives

M. Canle L. *, J.A. Santaballa, E. Vulliet

Chemical Reactivity and Photoreactivity Group, Department of Physical Chemistry and Chemical Engineering, University of A Coruña, Rúa Alejandro de la Sota, 1 E-15008 A Coruña, Galicia, Spain

Received 19 August 2004; received in revised form 15 April 2005; accepted 2 May 2005
Available online 8 June 2005

Abstract

Interaction between aromatic amines and TiO_2 takes place preferentially through the amino group when $pH > pK_a(BH^+)$ and, as a minor but mechanistically relevant mode, via a π-interaction if $pH < pK_a(BH^+)$. No significant direct photodegradation of aniline or *N*,*N*-dimethyl-aniline is detected in acidic medium using $\lambda > 290$ nm, but it is enhanced in alkaline medium. 2-Aminophenol and benzoquinone are the main photoproducts of direct irradiation of aniline. The main photoproducts of photocatalytic degradation of aniline at the pH of maximum adsorption are 2-aminophenol and phenol. Scavenging $HO^\bullet$ with *t*-BuOH shows that adsorbed aniline is oxidized by positive holes (h^+), with participation of the anilinium radical cation. In the case of *N*,*N*-dimethyl-aniline at the pH of maximum adsorption, *N*-methyl-aniline is the main photoproduct, formed also via the dimethyl anilinium radical cation. Photocatalytic degradation in acid medium is inhibited due to electrostatic repulsion between the positively charged surface and the protonated amines. Aniline is mainly transformed into phenol and 2-aminophenol, and *N*,*N*-dimethyl-aniline into aniline, that undergoes hydroxylation to phenol. In alkaline medium the main photoproduct of degradation of aniline is nitrobenzene, formed with involvement of the anilinyl radical.

Keywords: Adsorption; Aniline; Anilinium radical cation; Anilinyl radical; *N*,*N*-dimethylaniline; Heterogeneous photocatalysis; Photodegradation; Photoreactivity; Titanium dioxide

1. Introduction

Heterogeneous photocatalysis has been extensively investigated as a possible way for pollutants removal [1–3]. The physical basis of the method is the production of electron–hole (e^-–h^+) pairs by irradiation of a semiconductor with light having an energy equal to or greater than the band gap energy between its valence and conduction bands. In aerated aqueous systems, the photogenerated h^+ oxidize H_2O or HO^- at the surface of the semiconductor to produce $HO^\bullet$ radicals, as shown in the following equations:

$$H_2O_{ads} + h^+ \rightarrow HO^\bullet_{ads} + H^+ \quad (1)$$

$$HO^-_{ads} + h^+ \rightarrow HO^\bullet_{ads} \quad (2)$$

Electrons trapped at surface sites are removed by reduction of adsorbed O_2 to the superoxide radical anion, $O_2^{\bullet-}$, that may undergo protonation to its conjugated acid, $HO_2^\bullet$, as in Eqs. (3) [4] and (4) [5]:

$$O_{2\,ads} + e^- \leftrightarrows O^{\bullet-}_{2\,ads}, \quad E^0 = -0.33\ \text{V vs. NHE} \quad (3)$$

$$O_2^{\bullet-} + H^+ \leftrightarrows HO_2^\bullet, \quad pK_a(HO_2^\bullet) = 4.8 \quad (4)$$

In addition, the strong oxidant H_2O_2 is generated by dismutation of $O_2^{\bullet-}$ and $HO_2^\bullet$, Eq. (5) [6] and may then be reduced to $HO^\bullet$, as in Eq. (6) [7]:

$$O_2^{\bullet-} + HO_2^\bullet + H^+ \rightarrow H_2O_2 + O_2 \quad (5)$$

$$H_2O_2 + H^+ + e^- \rightarrow HO^\bullet + H_2O, \quad E^0 = -0.870\ \text{V vs. NHE} \quad (6)$$

* Corresponding author. Tel.: +34 981 167000; fax: +34 981 167065.
E-mail addresses: mcanle@udc.es (M. Canle L.), arturo@udc.es (J.A. Santaballa), vulliet@udc.es (E. Vulliet).

1010-6030/$ – see front matter © 2005 Elsevier B.V. All rights reserved.
doi:10.1016/j.jphotochem.2005.05.001

One of the questions often raised in photocatalysis concerns the nature of the oxidizing species involved in the photocatalytic process [8]. $HO^{\bullet}$ is regarded as the major species responsible for the degradation of organic pollutants, a hypothesis that is supported by the experimental observation of differences of several orders of magnitude between $[HO^{\bullet}]$ and $[O_2^{\bullet -}]$ upon irradiation of TiO_2 suspensions [9,10]. Indeed electronic spin resonance (ESR) spin-trapping studies have presented $HO^{\bullet}$ as the most abundant radical species in aqueous TiO_2 suspensions [11,12]. Furthermore, a large number of hydroxylated intermediates detected during the photocatalytic degradation of aromatic pollutants are consistent with a major action of $HO^{\bullet}$. Conversely, comparison of the quantum yield of $HO^{\bullet}$ and the photogenerated h^+ points to the oxidation process taking place mainly via h^+ and not via $HO^{\bullet}$ [13]. A competition $h^+/HO^{\bullet}$ has been reported for the herbicides 2,4-dichlorophenoxyacetic acid [14] and triclopyr [15]. Moreover, different regioselectivities of $HO^{\bullet}$ and h^+ have been evidenced in the transformation of 4-hydroxybenzylalcohol [16].

An on-going debate is whether the initial oxidation of the pollutant occurs on the surface of the catalyst or in the bulk of the solution. Indeed, it has been shown that $HO^{\bullet}$ can diffuse several hundred angstroms away from the surface into the bulk of the solution [17]. This statement was confirmed in the oxidation of furfuryl alcohol by $HO^{\bullet}$, for which a homogeneous-phase process is suggested [18]. On the other hand, ESR studies have established that $HO^{\bullet}$ might migrate only few atomic distances from the surface, and concluded that $HO^{\bullet}$ photooxidation is mostly a surface process [14].

Large amounts of aromatic amines can enter the aquatic environment as a consequence of the degradation of azo dyes [19,20] and nitrobenzenic compounds [21] or because they are formed as byproducts in combustion-related processes [22]. Acetanilide, phenylurea and carbamate-based pesticides can also produce aromatic amines, either by environmental degradation or by mammalian metabolism [23,24]. Many of these aromatic amines are known or suspected to be human or animal carcinogens [22]. Aniline and *N*,*N*-dimethyl-aniline can be considered as appropriate simple models of such compounds. Aniline is efficiently destroyed by heterogeneous photocatalysis with TiO_2, following a Langmuir–Hinshelwood kinetic model, both in suspensions [25–27] or with the catalyst immobilized on a support [28]. Synergetic effects of H_2O_2 [28] and O_3 [26] have been observed. Some hydroxylated compounds have been identified as products of transformation [25,27] and the formation of nitrobenzene has also been reported in alkaline medium [25].

To deepen our understanding of the role of adsorption and of the nature of the active species involved in the photocatalytic degradation of aromatic amines, the mechanism of degradation of aniline (A) and *N*,*N*-dimethyl-aniline (DMA) have been studied in TiO_2 suspensions. The process of adsorption on the catalyst, kinetics of disappearance and main degradation products and pathways have been studied at different pHs, and the contribution of direct degradation has also been evaluated.

Table 1
Relevant properties of the polymorphic phases of TiO_2 used

	Particle size (nm)	Average pore radius (nm)	Area ($m^2\,g^{-1}$)	pH_{PZC}
P25	30	Non-porous	50	6.3 [30]
Rutile	105	5.4	38	5.5 ± 0.8 [31]
Anatase	93	12.1	10	6.0 ± 0.9 [31]

2. Experimental

2.1. Materials and reagents

A and DMA (Aldrich) were purified by distillation under atmospheric pressure before use. All other chemicals were of analytical grade and used without further purification. The three TiO_2 powders used were anatase and rutile from Aldrich (99.8% and >99.9%, respectively), and Degussa P25 for which X-ray analysis indicated it was 80% anatase and 20% rutile. BET surface area and pore size distribution of the catalysts were determined by N_2 adsorption using a Sorptomatic Fisons 1900 system. Pore size distribution were obtained from desorption isotherm by the BJH method [29]. The particle size of rutile and P25 was obtained from the manufacturers, while for anatase it was determined using a Counter LS 230 granulometer. Some relevant properties of the different forms of TiO_2 used are summarised in Table 1.

2.2. Adsorption experiments

Adsorption experiments were conducted in the dark at room temperature. Isotherms were obtained using suspensions prepared by mixing solutions with different initial concentration of A or DMA with $2.5\,g\,L^{-1}$ of TiO_2 powder. In order to remove TiO_2 particles before analysis, the solutions were filtered through 0.45 μm cellulose nitrate membrane filters. The equilibrium concentration was determined by measuring the absorption of the corresponding UV peaks in solutions magnetically stirred during 1 h in the dark to attain the adsorption equilibrium. Absorption spectra were registered on a double beam Uvikon 941 plus spectrophotometer (Kontron Instruments) in Suprasil quartz cells of 1 cm optical path length. The pH of the filtered solutions at the concentration corresponding to the adsorption equilibrium was defined as the natural pH of the solution. The influence of pH on the adsorption was studied by adding HCl or KOH to the TiO_2 suspensions. pH measurements were carried out with a properly calibrated combined glass electrode.

2.3. Irradiation experiments

Irradiation experiments were carried out with a 750 mL Heraeus UV reactor system. The light source was a UV

medium-pressure Hg immersion lamp TQ 150, cooled by water flow. The temperature of the photoreactor was kept to within 298.0 ± 0.1 K. The irradiation spectrum was cut-off below 290 nm by inserting the lamp into a Duran 50 glass tube. Using the uranyl oxalate actinometer a mean photon flux of 1.41×10^{19} photon·s^{-1} attaining the solution was calculated applying the quantum yield $\Phi = 0.56$ [32]. Taking into account the absorption of TiO_2 Degussa P25, the number of photons potentially absorbable (per second) by TiO_2 was 5.8×10^{18}. The lamp was warmed up outside the reactor during 10 min prior to immersion into the suspension, already at the adsorption equilibrium.

2.4. Product analysis

The products were identified by comparison of their HPLC retention time and UV-spectrum with authentic standards, when available. Otherwise, LC–ES–MS was used. An HPLC Spectra System UV6000LP was used, with a Inertsil ODS-2 column (5 μm, 250 mm × 4.6 mm + precolumn). The mobile phase was a mixture $CH_3CO_2H/CH_3CO_2NH_4$ buffer (10 mM, pH 4.5)/MeCN in a ratio 60:40, with a flow rate of 1 mL min^{-1}. LC–ES–MS identification was carried out using an HP 1100-MSD system with ES and APCI sources. The ES mode was used under the following conditions: nebulizer pressure 50 psig, drying-gas (N_2) flow 13 L min^{-1}, drying-gas temperature 623 K, capillary voltage ±4000 V, fragment voltage 60 V. The APCI was used applying a 4 μA corona discharge.

3. Results and discussion

3.1. Adsorption on TiO_2

3.1.1. Isotherms at natural pH

The widely used photocatalyst Degussa P25 is predominantly in the polymorphic phase anatase. A series of experiments were carried out at natural pH and in the dark, in order to investigate the adsorption of A and DMA on anatase, rutile and P25 surfaces, with initial concentrations of amines varying from 3 to 250 μM. Changes in the pH of the suspension due to varying amine concentration were negligible with pH ca. 5.6 in P25 suspensions, and ca. 6.0 in rutile and anatase. Consequently, given the isoelectric points (pH_{PZC}) of the different polymorphic forms of TiO_2 used are statistically compatible with a value pH_{PZC} ca. 6 (Table 1) [30,31] and $pH < pH_{PZC}$, the surface of P25 bears slightly more positive charge than for rutile or anatase. The adsorption equilibrium was attained in less than 1 h. The isotherms representing the amount of adsorbed A per gram of photocatalyst (Q_{ads}) as a function of the concentration in the solution at the equilibrium (C_{eq}) are shown in Fig. 1. Noteworthy, although P25 is a mixture of rutile and anatase, the adsorption process is much more efficient for P25 than for a mixture of 80% anatase and 20% rutile in the same proportions. This may be understood

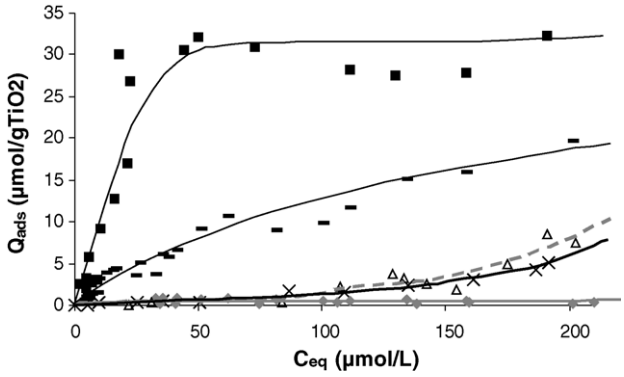

Fig. 1. Adsorption isotherms of A on: rutile (♦), anatase (△), P25 (▬), a mixture of 80% anatase + 20% rutile (×), and of DMA on P25 (■), all at natural pH. Tendency lines, shown only for the sake of clarity, are not mathematical fits.

in line with the explanation offered for the increase in the photocatalytic activity due to structural coupling of anatase and rutile in a bilayer form [33]. In the range of concentrations studied the adsorption on rutile is almost negligible, while the adsorption on anatase is very low until concentrations of ca. 100 μM are attained, and then increases progressively. In contrast, the amount adsorbed on P25 is much higher, with an isotherm that suggests a progressive coverage of the surface. In the case of DMA the adsorption is also favoured for P25, as compared to anatase and rutile, the isotherm on P25 (Fig. 1) suggesting a complete coverage of the surface at an adsorbed concentration $Q_{ads} \approx 30$ μmol (g TiO_2)$^{-1}$. The differences in adsorption between A and DMA are due to the structural and electronic differences between both compounds, but a detailed explanation of these is out of the scope of this paper.

The adsorption is not proportional to the specific area of the catalyst Table 1, but related to the particle size of the three TiO_2 powders. The stronger adsorption on P25 may be attributed to its acidity, that makes the TiO_2 surface slightly positive, and therefore more prone to interaction with the non-bonding e^- of the nitrogen atoms of A and DMA ($pK_a(BH^+) = 4.65$ for A, 5.07 for DMA) under conditions of natural pH (vide supra, Section 2) [34].

Since the most favourable adsorption process was, by far, observed for P25 with both A and DMA, we decided to use this catalyst in the rest of this study. The high photocatalytic activity of P25 is attributed to the increase in charge-separation efficiency resulting from interfacial e^--transfer from anatase to rutile, that are coupled in a bilayer form [33].

3.1.2. Influence of the pH on the adsorption

The influence of the pH on the adsorption has been investigated, considering that pH_{PZC} (TiO_2) ca. 6.3 [30]. Fig. 2 shows the pH of the medium is critical for the adsorption of both A and DMA. The bell-shaped dependences observed show the combined influences of the protonation of the aromatic amines and of TiO_2 surface. The observed maxima correspond to the arithmetic mean of $pK_a(BH^+)$ of the

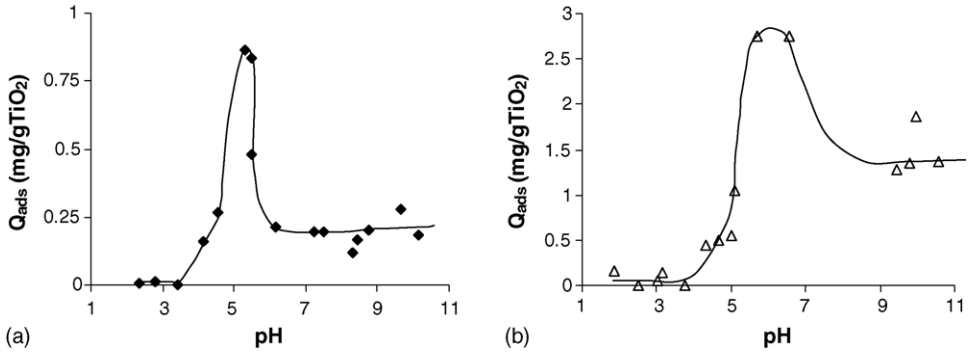

Fig. 2. Amount of (a) A ($C_0 = 49.5\,mg\,L^{-1}$), and (b) DMA ($C_0 = 73.6\,mg\,L^{-1}$) adsorbed per gram of TiO_2 P25 as a function of the pH. Tendency lines, shown only for the sake of clarity, are not mathematical fits.

amines and pH_{PZC}. For 3.5 < pH only a very low adsorption is detected. When 3.5 < pH < 5.5 the adsorption increases with pH to reach a maximum at pH values of ca. 5.5 and 5.7 for A and DMA, respectively. These pH values are referred to as pH_{ads} in what follows.

These results indicate that the main interaction between A and DMA and the surface of the catalyst takes place through the amino group, rather than via a π-interaction with the aromatic ring, that constitutes a minor, but relevant, mode of interaction (vide infra, Section 3.3.1). Indeed, in acidic medium the non-bonding electron pair of the nitrogen atom is not available to establish this coordinative interaction, resulting in low adsorption. The adsorbed quantity is maximum when $pK_a(BH^+)$ (=4.65 for A, 5.07 for DMA) [34] < pH < pH_{PZC} (TiO_2). Under these conditions, the interactions between the slightly positively charged surface of TiO_2 and the non-bonding electron pair of the nitrogen are optimal. In this pH interval, 50% of A in the solution is adsorbed, and 75% of DMA. When pH > pH_{PZC} (TiO_2) the adsorbed quantities decrease rapidly. In this case the surface of TiO_2 is slightly negatively charged, and the coordinative interactions with the amino groups are reduced. On the other hand, the potential competition between Cl^- and A/DMA for the active sites on the surface contribute to lower the adsorption at low pH values [35].

3.2. Direct degradation

A and DMA show significant absorption for λ < 320 nm, with maxima at λ = 230 and 282 nm for A and λ_{max} = 244 nm and a shoulder at λ = 282 nm for DMA, therefore direct photodegradation may take place despite the fact that the Duran 50 glass tube used cuts-off essentially all light below 290 nm (Fig. 3).

No significant degradation has been detected in acid medium where A and DMA are fully protonated. This is partly because the absorption of the protonated forms is low as compared to their respective conjugate bases (ε (λ = 282 nm, pH = 10.9) = 1600 L mol^{-1} cm^{-1}, while ε (λ = 282 nm, pH = 3.0) = 200 L mol^{-1} cm^{-1} for A). On the other hand, short-lived species formed from protonated A and DMA are expected to be less stable than the corresponding conjugate bases [36].

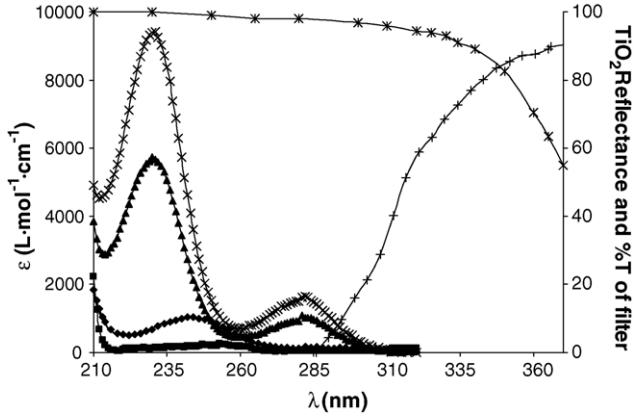

Fig. 3. Absorption spectra of A and DMA at different pHs (■ A, pH = 2.9; ▲ A, pH = 5.5; × A, pH = 10.9; ♦ DMA, pH = 5.7), reflectance spectra of TiO_2 (*) and % of transmittance of the Duran glass filter (+).

Photodegradation processes observed in mildly acidic and basic medium followed pseudo-first order kinetics according to $C = C_0\,e^{-k_{app}t}$, where C is the concentration of amine in solution, C_0 the initial concentration of amine, and k_{app} the apparent rate constants, collected in Table 2 for A (pH_{ads} = 5.5 and pH = 10.9) and DMA (pH_{ads} = 5.7). From the measured rate constants, direct degradation is almost negligible as compared with photocatalyzed photodegradation (vide infra). This should be attributed to the low absorption of aniline under the experimental conditions (as stated above, the irradiation spectrum was cut-off below 290 nm by inserting the

Table 2
Apparent rate constants for direct and photocatalyzed photodegradation of A and DMA at different pH values

	k_{app} (min^{-1})				
	Direct degradation		Photocatalysis		
	pH_{ads}	pH = 10.9	pH = 3	pH_{ads}	pH = 11.6
A	0.002	0.086	0.034	0.069	0.098
DMA	0.007		0.012	0.044	

lamp into a Duran 50 glass tube). The increased photoreactivity in alkaline medium may have its origin on the differences of absorption spectra in alkaline medium and at pH_{ads}. On the other hand, when $pH = pH_{ads}$, the photodegradation takes place to a lower extent: less than 25% of the initial A is degraded after 2 h, and about 55% in the case of DMA.

2-Aminophenol (2APh) and benzoquinone (BQ) were unambiguously identified as photoproducts of A by comparison with authentic samples. A third photoproduct with retention time corresponding to 4-aminophenol (4APh) was also observed. In the absence of photocatalytically generated $HO^{\bullet}$ radicals, 2APh and 4APh must arise from hydrolysis (preferentially at position C_2) of a sufficiently long-lived excited state generated upon direct irradiation. The presence of BQ points to a direct photoionization process leading to the anilinium radical cation [37] that then reacts with water to yield phenol (Ph) and, eventually, BQ. Under the irradiation conditions, photoionization is a multiphotonic process [38,39] which provides additional support to neglect direct photodegradation as compared to photocatalyzed photodegradation.

During the direct photodegradation of A in alkaline medium the solution passed rapidly from colourless to brown, and the HPLC analysis evidenced the formation of five products, for which the retention times were twice to eight times longer than that of A, pointing to a polymerization process. One of these products exhibited a mass in agreement with the structure of azobenzene (AB, $m/z = 182$). Traces of nitrobenzene (NB) were also found as photoproduct. These products are in agreement with a direct photoionization process to the anilinium radical cation [37] followed by deprotonation to the anilinyl radical and N–N coupling to yield AB, or oxidation to NB.

3.3. Photocatalytic degradation

In a suspension of TiO_2, the photocatalytic decomposition rate can be written according to the Langmuir–Hinshelwood kinetic model independently of the location of the reactants on the surface of the catalyst or in the bulk of the solution[17]. At low concentration of substrate the reaction rate approximates a first-order kinetic law, according to $-dC_{eq}/dt = k_{app}C_{eq}$, where k_{app} is the apparent degradation constant, including the reaction rate constant and the adsorption equilibrium and/or diffusion coefficients. The influence of pH on the photocatalytic degradation was studied by comparison of the different k_{app} obtained under different initial pH conditions (Table 2). A and DMA were preliminary adsorbed in the dark during 1 h to reach the equilibrium concentration, C_{eq}. The presence of NaCl 10 mM has been reported to induce no modification in the photocatalytic degradation of A [14] which led us to assume that the addition of low salt concentrations does not affect the photocatalytic process. Considering the concentration of TiO_2 in suspension ($2.5\,g\,L^{-1}$), all the available photons are presumed to be absorbed by the catalyst. The rates of photodegradation of A and DMA have been measured in strong acidic solution and for $pH = pH_{ads}$ (5.5 and 5.7 for A and DMA, respectively). A has also been irradiated in an alkaline suspension of TiO_2.

3.3.1. Photocatalytic degradation at pH_{ads}

The time evolution of A and DMA (right ordinate axis) and of the main photoproducts (left ordinate axis) formed under irradiation at pH_{ads} is shown in Fig. 4.

The main photoproducts found for A are 2APh and Ph. Unexpectedly, 4APh is not detected. Hydroxylation takes place in *ortho*- with respect to the $–NH_2$ group, leading to 2APh, in spite of the lower steric hindrance of the *para*-position. BQ and NB are also detected. Traces of benzidine (BZ) have been identified with maximum concentration ca. 0.05 μM. A sixth product with $m/z = 124$, corresponding to a trihydroxybenzene is detected. The formation of hydroxyhydroquinone has been reported during the photocatalytic and electrochemical degradation of A [21] and, from our HPLC and LC–ES–MS results, we identify this as 1,2,4-trihydroxybenzene (HHQ).

When irradiated in the presence of 100 mM *t*-BuOH, used as $HO^{\bullet}$ quencher [40] the degradation rate of A was reduced by 85%. In this case the formation of 2APh was completely inhibited, and no trace of NB detected. Besides, the forma-

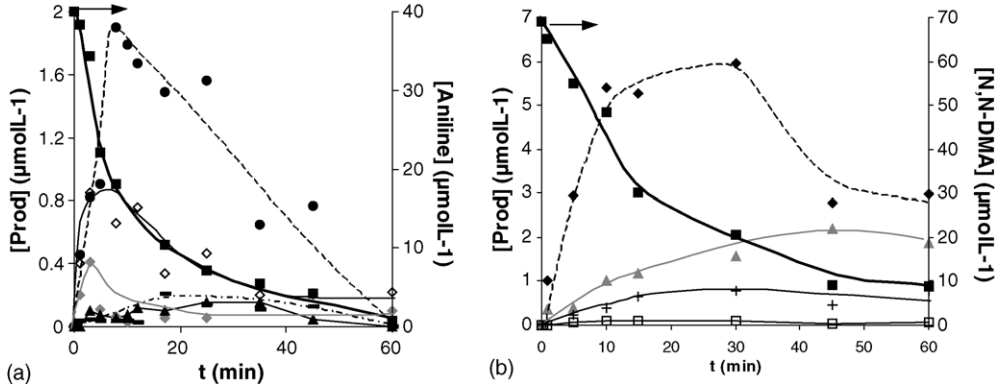

Fig. 4. Time evolution of the products formed during the degradation of (a) A (■, A; ●, 2APh; ▬, BQ; ◊, Ph; ▲, HHQ; ◆, NB), pH = 5.5, and (b) DMA (□, DMA; ▲, MA; ■, A; +, 3-HO-MA; △, 4-HO-MA), pH = 5.7. Tendency lines, shown only for the sake of clarity, are not mathematical fits.

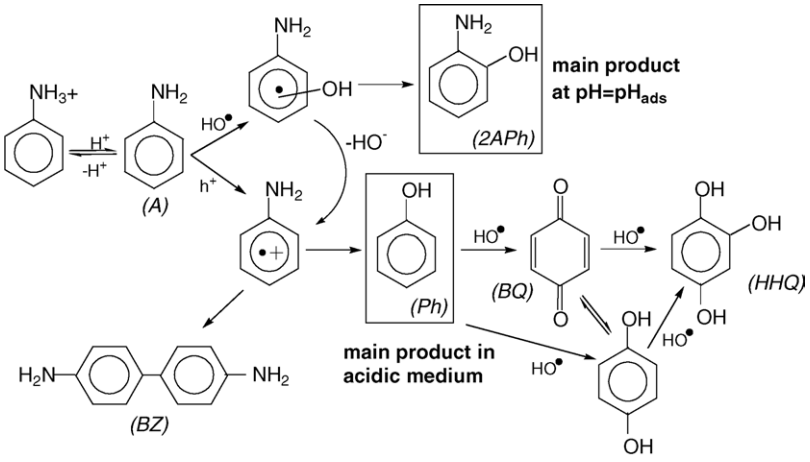

Scheme 1. Mechanism of generation of the main photoproducts found during the photocatalytic degradation of A at pH_{ads} and acidic pH.

tion of Ph was favoured and BQ also observed. These results show the involvement of different oxidizing species in the degradation, according to Scheme 1.

Since the strongly oxidizing radical $HO^{\bullet}$ typically reacts by addition [41,42] in its presence the oxidation of A leads mainly to the corresponding hydroxycyclohexadienyl radicals [37]. The $HO^{\bullet}$-adduct may either be rapidly transformed into 2APh or produce the anilinium radical cation by a subsequent elimination of HO^{-}.

In the absence of $HO^{\bullet}$, the degradation may result from a reaction with h^+ or $HO_2^{\bullet}/O_2^{\bullet-}$. However, as the reaction of A with $HO_2^{\bullet}$ has been shown to produce NB [43] Ph must result from the oxidation of A by h^+, leading to the anilinium radical cation/anilinyl radical. Hydrolysis on the C adjacent to the nitrogen (C_1), with subsequent elimination of the amino group and formation of ammonia or nitrate ions [28] leads to Ph. Formation of Ph has been previously reported during the degradation of A by photocatalytic [24] electro-Fenton or photoelectro-Fenton processes [26] but not during the classical Fenton reaction [39].

Our adsorption studies point (vide supra, Section 3.1.2) to a preferential interaction between the amino group of A and DMA and the surface of the catalyst when $pH > pK_a(BH^+)$. However, the mechanism of direct oxidation by h^+ just described requires preliminary adsorption of the molecule on the surface of the catalyst and seems more favourable when the adsorption on the surface of the catalyst takes place via a π-interaction with the aromatic ring (vide supra, Section 3.1.2). This becomes necessarily the mode of interaction with the surface of the photocatalyst as pH approaches $pK_a(BH^+)$ and the amino group gets protonated. Under such conditions Ph is the main photoproduct (Scheme 1). It has been proposed that the electronic properties of TiO_2 surface change upon irradiation, altering the adsorption sites [44]. We can therefore hypothesize that minute light-induced modifications of the orientation of the molecule with respect to the surface are possible. Thus, a more vertical orientation of the adsorbed molecules, with C_4 pointing to the surface and the amino group slightly upwards, may be supported by the fact that hydroxylation of the ring is detected only in *ortho*- position.

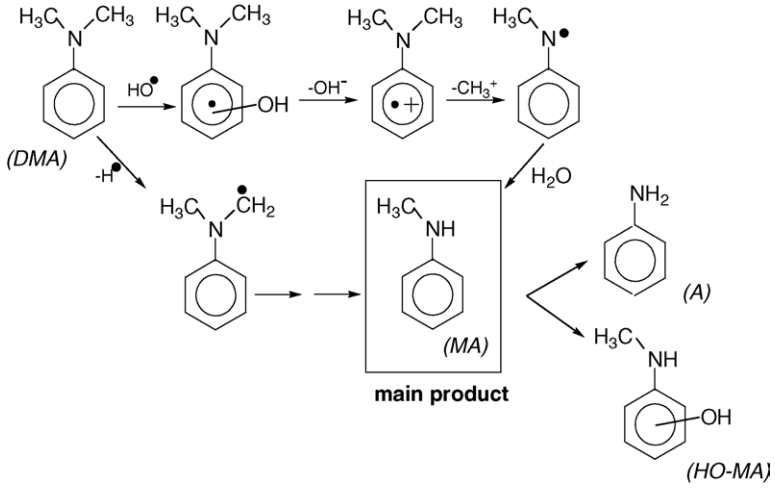

Scheme 2. Mechanism of generation of the main photoproducts found during the photocatalytic degradation of DMA at pH_{ads}.

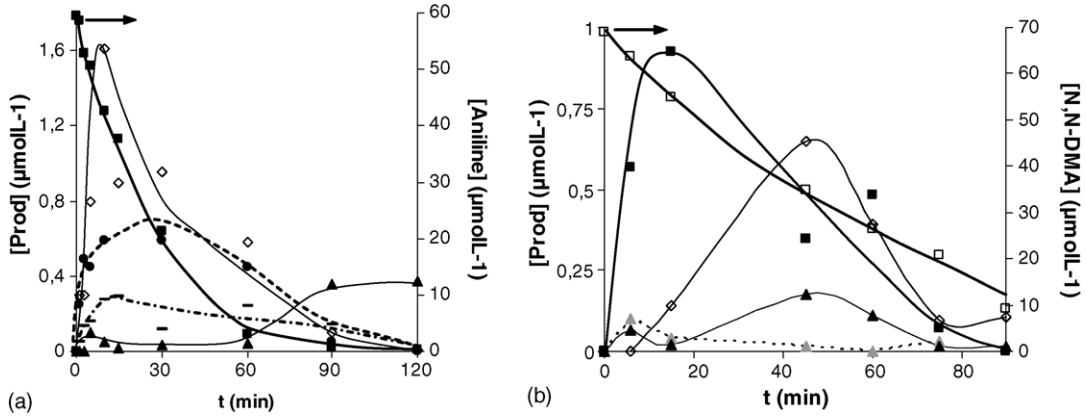

Fig. 5. Time evolution of the products formed during the degradation of (a) A (■, A; ●, 2APh; ▬, BQ; ◊, Ph; ▲, HHQ) and (b) DMA (□, DMA; ▲, MA; ■, A; ◊, Ph; ▲, HHQ), both at pH = 3. Tendency lines, shown only for the sake of clarity, are not mathematical fits.

The presence of BZ as a photoproduct indicates also a bimolecular reaction between the anilinium/anilinyl radicals [37] supporting the hypothesis of a change in the orientation of the molecule.

When irradiated at pH_{ads} DMA undergoes demethylation, leading to *N*-methylaniline (MA) as main photoproduct (Fig. 4). $HO^{\bullet}$ is known to react with DMA by addition to the aromatic ring leading to the hydroxycyclohexadienyl radical and, by hydrogen abstraction from one methyl group, to the corresponding C-centered radical [45] as shown in Scheme 2.

In the first case the $HO^{\bullet}$-adduct is rapidly transformed into a radical cation, leading to demethylation. Only a low signal in HPLC–MS analyses corresponding to a product with the m/z = (DMA + 16) has been detected, suggesting ring hydroxylation is a minor route. MA may subsequently demethylate to A, or undergo hydroxylation, as proved by the presence of three hydroxy-*N*-methyl-aniline isomers, only two of which have been quantified: 3-hydroxy-*N*-methylaniline (3-HO-MA) and 4-hydroxy-*N*-methylaniline (4-HO-MA), as shown in Fig. 4.

3.3.2. Photocatalytic degradation in acid medium

Both for A and DMA the rate of photocatalytic decomposition decreases at low pH values (Table 2), as the electrostatic repulsion between the positively charged surface and the protonated molecules, as well as the competitive adsorption of the acid counter-anion (Cl^{-}) limit the possibilities of contact between A and DMA and the adsorbed active species. Nevertheless, the photocatalytic rates are only partially reduced (50 and 75% for A and DMA respectively) with respect to the pH conditions described above. This is in agreement with the previous suggestion (vide supra, Sections 3.1.2 and 3.3.1) that A interacts with the surface through its π-system in acid medium. The time evolution of A and DMA (right ordinate axis) and of the main photoproducts (left ordinate axis) formed upon irradiation in acid medium is shown in Fig. 5.

A is rapidly transformed into Ph and 2APh. BQ is also formed in a significant concentration and HHQ appears after 60 min of irradiation. Small quantities of BD are also detected. As above, 2APh is the single isomer detected, 4APh not being found.

Under acid conditions DMA is directly transformed into A, and only small quantities of MA are observed (Fig. 5). Ph is also produced, presumably from subsequent degradation of A, from which HHQ is also derived (vide supra, Section 3.3.1).

3.3.3. Photocatalytic degradation in alkaline medium

The transformation of A in alkaline medium is the fastest (Table 2). Indeed, under this pH conditions the formation of $HO^{\bullet}$ by oxidation of HO^{-} by the photogenerated h^{+} becomes favoured [5]. The time evolution of A (right ordinate axis) and of the main photoproducts formed (left ordinate axis) is shown in Fig. 6.

No trace of 2APh is detected, and the formation of Ph is only a very minor route. Noteworthy, under these condi-

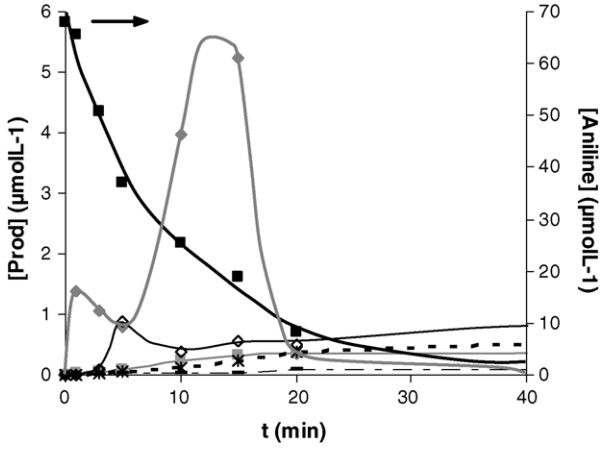

Fig. 6. Time evolution of the products formed during the degradation of A in alkaline medium (■, A; ◆, NB; ◊, Ph; ▬, BQ; ■, 3-NPh; *, 4-NPh) at pH = 11.6. Tendency lines, shown only for the sake of clarity, are not mathematical fits.

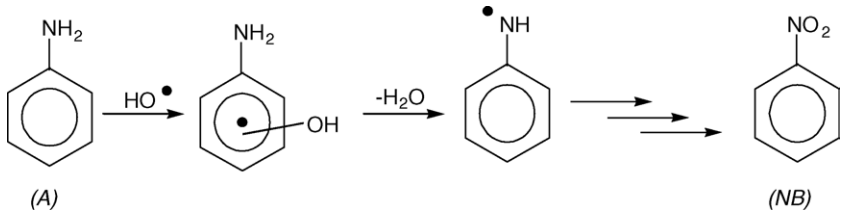

Scheme 3. Mechanism of generation of nitrobenzene (NB) during the photocatalytic degradation of A in alkaline medium.

tions only traces of one of the coloured compounds produced during the non-catalyzed direct degradation are detected, confirming that TiO_2 behaves as an internal filter for the direct degradation. Formation of the main observed photoproduct, NB, has been reported during the electro-Fenton and photoelectro-Fenton degradation of A [27]. It was proposed that the process was initiated by $H^\bullet$ abstraction from the deprotonated amino group, followed by oxidation of the resulting radical by $HO_2^\bullet$, in contrast with the selective attack of $HO_2^\bullet$ on the amino group during the electrochemical degradation of A [43]. However, in photocatalytic processes $HO^\bullet$ has suggested to be the main oxidizing species in alkaline medium [9,46] and no NB is found at pH_{ads} in the presence of *t*-BuOH. Moreover, $HO^\bullet$ is known to react mainly by addition and not by abstraction of $H^\bullet$ from aniline [37,42]. Consequently, NB must arise from addition of $HO^\bullet$ to the aromatic ring, followed by elimination of HO^- from the $HO^\bullet$-adduct and deprotonation of the radical cation to form the anilinyl radical, that is further oxidized to NB (Scheme 3) [43].

3-Nitrophenol (3-NPh) and 4-nitrophenol (4-NPh), that are also found as minor photoproducts, must arise by $HO^\bullet$ addition to NB. Ph and BQ, also observed as minor photoproducts, are generated via oxidation by the photogenerated h^+, as in Scheme 1.

4. Conclusions

Adsorption of A and DMA onto Degussa P25 is much more efficient than on anatase or rutile, or on a mixture of both. The extent of adsorption is not proportional to the specific area of the catalyst, but related to the particle size and acidity of the photocatalyst. The pH is critical, the adsorption reaching a maximum at a pH_{ads}, that corresponds to the arithmetic mean of $pK_a(BH^+)$ and pH_{PZC}. The interaction between the aromatic amines and the surface appears to take place preferentially through the unprotonated amino group when $pH > pK_a(BH^+)$ and, as a minor but mechanistically relevant interaction mode, via a π-interaction in acid medium when $pH < pK_a(BH^+)$.

No significant direct degradation of A or DMA is detected in acidic medium. Conversely, direct photodegradation is enhanced in alkaline medium. 2-APh, and BQ were identified as main photoproducts of direct irradiation of A. AB, NB and different unidentified polymerization products were found as minor photoproducts of direct irradiation.

The main photoproducts found upon photocatalytic degradation of A at pH_{ads} are 2-APh and Ph, with BQ, NB, BD and HHQ as minor photoproducts. Scavenging of $HO^\bullet$ with *t*-BuOH led to a strong reduction of the reaction rate and to the disappearance of 2-APh and NB as photoproducts, showing that adsorbed A is oxidized by h^+ to yield the anilinium radical cation. In the case of DMA at pH_{ads}, MA is the main photoproduct, evidencing the involvement of the anilinium radical cation, that undergoes C–N fragmentation. MA undergoes further demethylation to A or hydroxylation, leading to 3-HO-MA and 4-HO-MA.

Photocatalytic degradation in acidic medium is inhibited due to electrostatic repulsion between the positively charged surface and the protonated amines. A is transformed into Ph and 2-APh, with BQ and HHQ as minor photoproducts. DMA is transformed into A, that undergoes hydroxylation to Ph, MA being also observed.

Photocatalytic degradation in alkaline medium is fast. The main photoproduct of A is NB, indicating the involvement of the anilinyl radical. Accordingly, only traces of Ph are observed.

Acknowledgements

This work was carried out with financial support from research project PGIDTO2TAM10301PR (*Xunta de Galicia*, Spain). EV acknowledges the *Université Claude Bernard Lyon I* (France) for a leave of absence and the Universidade da Coruña (Spain) for supporting a postdoctoral stay. The authors thank M. Fernand Chassagneux (L.M.I. *Université Claude Bernard Lyon I*) for technical support in BET surface area measurements, and also Degussa for kindly supplying samples of P-25 TiO_2. Finally, we acknowledge the useful and constructive comments of the referees.

References

[1] N. Serpone, E. Pelizzetti (Eds.), Photocatalysis: Fundamentals and Applications, Wiley, New York, 1989.
[2] D.W. Bahnemann, J. Cunningham, M.A. Fox, E. Pelizzetti, P. Pichat, N. Serpone, G.R. Helz, R.G. Zepp, D.G. Crosby (Eds.), Surface and Aquatic Photochemistry, Lewis Publishers, Boca Ratón, 1993.

[3] M. Kaneko, I. Okura (Eds.), Photocatalysis: Science and Technology, Springer-Verlag, Berlin, 2002.
[4] Y. Sawada, T. Iyanagi, I. Yamazaki, Biochemistry 14 (1975) 3761.
[5] B.H.J. Bielski, D.E. Cabelli, R.L. Arudi, A.B. Ross, J. Phys. Chem. Ref. Data 14 (1985) 1041.
[6] B.H.J. Bielski, Photochem. Photobiol. 28 (1978) 645.
[7] W.H. Koppenol, J. Butler, Adv. Free Radical Biol. Med. 1 (1985) 91.
[8] C. Minero, V. Maurino, E. Pelizzetti, in: V. Ramamurthy, K.S. Schanze (Eds.), Semiconductor Photochemistry and Photophysics, Marcel Dekker, New York, 2003, p. 211.
[9] P.F. Schwarz, N.J. Turro, S.H. Bossmann, A.M. Braun, A.-M.A.A. Wahab, H. Dürr, J. Phys. Chem. B 101 (1997) 7127.
[10] Y. Nosaka, Y. Yamashita, H. Fukuyama, J. Phys. Chem. B 101 (1997) 5822.
[11] C.D. Jaeger, A.J. Bard, J. Phys. Chem. 83 (1979) 3146.
[12] E.M. Ceresa, L. Burlamacchi, M. Visca, J. Mater. Sci. 18 (1983) 289.
[13] K. Ishibashi, A. Fujishima, T. Watanabe, K. Hashimoto, J. Photochem. Photobiol. A: Chem. 134 (2000) 139.
[14] L. Sun, K.M. Schindler, A.R. Hoy, J.R. Bolton, G.R. Helz, R.G. Zepp, D.G. Crosby (Eds.), Aquatic and Surface Photochemistry, Lewis Publishers, Boca Ratón, 1994, p. 409.
[15] I. Poulios, M. Kositzi, A. Kouras, J. Photochem. Photobiol. A: Chem. 115 (1998) 175.
[16] C. Richard, J. Photochem. Photobiol. A: Chem. 72 (1993) 179.
[17] C.S. Turchi, D.F. Ollis, J. Catal. 122 (1990) 178.
[18] C. Richard, J. Lemaire, J. Photochem. Photobiol. A: Chem. 55 (1990) 127.
[19] R.F. Straub, R.D. Boyksner, J.T. Keever, J. Anal. Chem. 65 (1993) 2131.
[20] I.K. Konstantinou, T.A. Albanis, Appl. Catal. B: Environ. 49 (2004) 1.
[21] F.M. Dunnivant, R.P. Schwarzenbach, D.L. Macalady, Environ. Sci. Technol. 26 (1992) 2133.
[22] Committee on Amines. Board on Toxicology and Environmental Health Hazards, Aromatic Amines: An Assesment of the Biological and Environmental Effects, Assenbly of Life Sciences National Research Council, National Academic Press, Washington, DC, 1981.
[23] T. Roerts, D.H. Hutson, P.J. Jewess, P.W. Lee, P.H. Nicholls, J.R. Plimmer (Eds.), Metabolic Pathways of Agrochemicals. Part 2. Insecticides and Fungicides, The Royal Society of Chemistry, Cambridge, 1999.
[24] H. Burrows, M. Canle L, J.A. Santaballa, J. Photochem. Photobiol. B: Biol. 67 (2002) 71.
[25] L. Sánchez, J. Peral, X. Domènech, Electrochim. Acta 42 (1997) 1877.
[26] L. Sánchez, J. Peral, X. Domenech, Appl. Catal. B: Environ. 19 (1998) 59.
[27] E. Brillas, E. Mur, R. Sauleda, L. Sánchez, J. Peral, X. Domenech, J. Casado, Appl. Catal. B: Environ. 16 (1998) 31.
[28] L. Wenhua, L. Hong, C. Sao'an, Z. Jianqing, C. Chunan, J. Photochem. Photobiol. A: Chem. 131 (2000) 125.
[29] E.P. Barrett, L.G. Joyner, P.P. Halenda, J. Am. Chem. Soc. 73 (1951) 373.
[30] N. Jaffrezic-Renault, P. Pichat, A. Foissy, R. Mercier, J. Phys. Chem. 90 (1986) 2733.
[31] M. Kosmulski, Adv. Coll. Interf. Sci. 99 (2002) 255.
[32] A.M. Braun, M.T. Maurette, E. Oliveros, Technologie Photochimique, Presses Polytechniques, Romandes, Lausanne, 1986, pp. 70–77.
[33] T. Kawahara, Y. Konishi, H. Tada, N. Tohge, J. Nishii, S. Ito, Angew. Chem. Int. Ed. 41 (2002) 2811.
[34] F.E. Condon, J. Am. Chem. Soc. 87 (1965) 4485.
[35] S. Tanaka, U.K. Saha, Wat. Sci. Technol. 9 (1994) 47.
[36] M. Canle L., J.A. Santaballa, S. Steenken, Chem. Eur. J. 5 (1999) 1192.
[37] L. Qin, G.N.R. Tripathi, R.H. Shculer, Z. Naturforsch. 40a (1985) 1026.
[38] F. Saito, S. Tobita, H. Shizuka, J. Chem. Soc., Faraday Trans. 92 (1996) 4177.
[39] F. Saito, S. Tobita, H. Shizuka, J. Photochem. Photobiol. A: Chem. 106 (1997) 119.
[40] G.V. Buxton, C.L. Greenstock, W.P. Helman, A.B. Roos, J. Phys. Chem. Ref. Data 17 (1988) 513.
[41] M.E.D.G. Azenha, H.D. Burrows, M. Canle L, R. Coimbra, M.I. Fernández, M.V. García, A.E. Rodrígues, J.A. Santaballa, S. Steenken, Chem. Commun. (2003) 112.
[42] S. Steenken, J. Chem. Soc., Faraday Trans. 1 83 (1987) 113.
[43] E. Brillas, R.M. Bastida, E. Llosa, J. Electrochem. Soc. 142 (1995) 1733.
[44] Y. Xu, C.H. Langford, J. Photochem. Photobiol. A: Chem. 133 (2000) 67.
[45] J. Holcman, K. Sehested, J. Phys. Chem. 81 (1977) 1963.
[46] C. Richard, P. Boule, J. Photochem. Photobiol. A: Chem. 60 (1991) 235.